Propagation of Localization Instability Under Active and Passive Loading

Ronaldo I. Borja[1] and Timothy Y. Lai[2]

Abstract: The mechanical response of a solid continuum changes drastically as the deformation evolves from a diffuse state to a highly localized state. For this reason the subject of strain localization has received much research attention lately. This paper investigates the impact of strain localization in the form of strong discontinuity, or displacement jump, on the limit strengths of retaining walls supporting an elastoplastic backfill. The analysis focuses on the propagation of strong instability in active and passive loading using a recently developed strong discontinuity finite element model where the elements are enhanced to accommodate the presence of displacement jumps. Specifically, the analysis applies to dilative frictional material that is susceptible to shear banding. For the retaining wall problem, strong instability is shown to initiate at the ground surface and propagate downward at an angle that depends on the state of stress at the onset of localization.

DOI: 10.1061/(ASCE)1090-0241(2002)128:1(64)

CE Database keywords: Constitutive models; Finite element method; Limit analysis; Banding; Plasticity; Localization; Strain distribution; Retaining walls.

Introduction

Material instability is generally regarded as a precursor to failure in geomaterials. It manifests itself in the form of a shear band, a narrow zone of intense shearing to which most softening phenomena are attributed (Rudnicki 1977; Aydin and Johnson 1978; Pietruszczak and Mróz 1981; Read and Hegemier 1984; Viggiani et al. 1994; Labuz et al. 1996). Strain localization occurs in geomaterials under various stress conditions, from the simple case of uniaxial compression of cyclindrical soil and rock specimens, to behavior as complex as those encountered in the hydraulic fracturing of rocks. Thus, it is important to be able to predict when a shear band forms and how this zone of intense deformation is oriented within the material.

Much research effort has focused lately on developing mathematical and numerical models for capturing experimentally observed strain localization phenomena where the zone of intense shearing has a finite and measurable characteristic thickness. Such zone of localized deformation is termed ''weak discontinuity'' in the general literature. In many instances, the shear band may have an infinitesimal thickness in the sense that the specimen practically experiences a displacement jump, termed ''strong discontinuity'' by Simo et al. (1993). Regardless of whether the shear band has a zero or a finite thickness, strain localization remains an intriguing problem that has attracted much research attention due to the difficulty in capturing the phenomenon with available conventional modeling techniques. This has led to the development of special models and less conventional numerical approaches, such as those based on nonlocal models (Bazant and Pijaudier-Cabot 1988; Adachi et al. 1991), element breaking (Wan et al. 1980), gradient plasticity (de Borst and Mühlhaus 1992; de Borst et al. 1995; Oka et al. 2000), adaptive remeshing techniques (Zienkiewicz et al. 1995), and element enhancements (Ortiz et al. 1987; Larsson et al. 1993; Simo et al. 1993; Armero and Garikipati 1995), among others.

For dense frictional materials it is well known that the residual strength at large deformation is generally lower than the peak strength. This implies that some strain softening must occur following the peak strength. The softening response is usually accompanied by localized deformation (Perić et al. 1992; 1993). The goal of this article is to investigate and model this strain softening response as a problem of material instability. Specifically, we outline precise conditions for the onset of strong discontinuity and follow the evolution of the slip surface until the structure is brought to a final residual stress state.

Within the framework of the finite element (FE) method, an important consideration in modeling strain localization phenomena is that the solution must be objective with respect to mesh refinement and insensitive to element alignment. In addition, the theoretical localization model must be well formulated so that length-scale issues are properly resolved. Here, we adopt a strong discontinuity formulation and devise a FE approximation in which the elements are enhanced to allow an accurate resolution of highly localized deformation patterns. Recent results have shown that this approach can indeed provide mesh-independent FE solutions (Reguerio and Borja 1999; Borja 2000; Borja et al. 2000; Borja and Reguerio 2001; Regueiro and Borja 2001).

A classic manifestation of strain localization in geotechnical application occurs behind a retaining wall in the form of slip surfaces. For horizontal loose sandy backfill supported by a smooth vertical wall, Rankine's (1857) theory predicts that all

[1]Associate Professor, Dept. of Civil and Environmental Engineering, Terman Engineering Center, Stanford Univ., Stanford, CA 94305-4020. E-mail: borja@stanford.edu

[2]Graduate Student, Dept. of Civil and Environmental Engineering, Stanford Univ., Stanford, CA.

Note. Discussion open until June 1, 2002. Separate discussions must be submitted for individual papers. To extend the closing date by one month, a written request must be filed with the ASCE Managing Editor. The manuscript for this paper was submitted for review and possible publication on September 6, 2000; approved on March 23, 2001. This paper is part of the ***Journal of Geotechnical and Geoenvironmental Engineering***, Vol. 128, No. 1, January 1, 2002. ©ASCE, ISSN 1090-0241/2002/1-64–75/$8.00+$.50 per page.

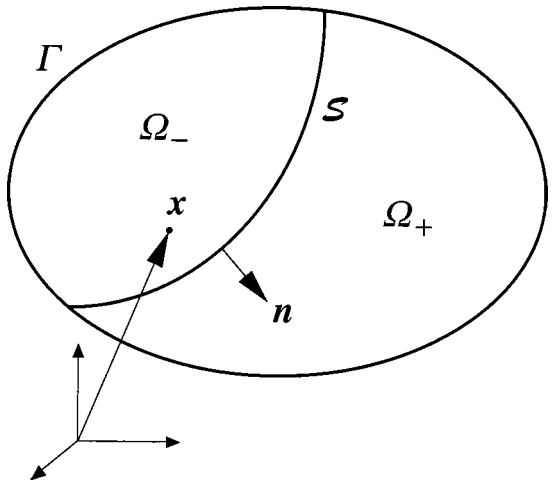

Fig. 1. Elastoplastic continuum cut by a shear band

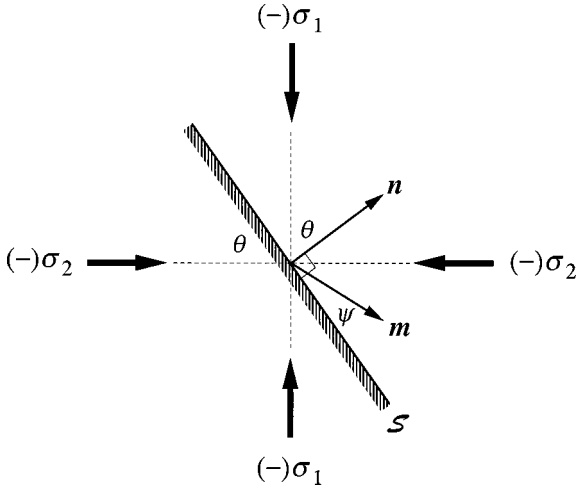

Fig. 2. Orientation of surface of discontinuity $\mathcal{S}$ and unit vectors **m** and **n**

points in the backfill will yield at the same time when either horizontally stretched (active loading) or horizontally compressed (passive loading). In this case, a slip plane at failure theoretically can pass through any point in the continuum. Rankine considered yielding and failure to be synonymous—the formation of slip surface is dictated by the satisfaction of a yield or failure criterion, and not by any material instability consideration. However, such an approach may not necessarily hold for the case of dense granular backfill.

In this article we reanalyze the retaining wall problem using the strong discontinuity formulation and treat the backfill as an elastoplastic, dilatant frictional material susceptible to localized deformation instability. More specifically, we assume a nonassociated Drucker-Prager model for the continuum and investigate the onset of strong discontinuity, or displacement jump, in active and passive loading. Due to a nonuniform stress field resulting from the presence of gravity loads, localization in the continuum takes place progressively, rather than simultaneously, starting from the most critically stressed points and propagating in the direction favoring material bifurcations (Rudnicki and Rice 1975; Runesson et al. 1991; Borja 2002a). We show that the localization condition for the retaining wall problem is first satisfied at the ground surface, allowing displacement jumps to emerge. Then the displacement discontinuity, or slip line, propagates downward at an angle that depends on the state of stress—active or passive—at which the localization condition is first satisfied. This contrasts with the Rankine theory which states that failure at all points occurs simultaneously in a loose, homogeneous granular backfill.

Localization Theory

Consider an elastic-perfectly plastic continuum deforming homogeneously as shown in Fig. 1. Assume that the constitutive response prior to localization is described by a yield function F and a plastic potential function Q, and let c^e_{ijkl} denote the component of the elastic tangential moduli tensor having the properties of major and minor symmetries, as well as positive definiteness. We identify two modes of shear band bifurcation instability: continuous bifurcation and discontinuous bifurcation. In continuous bifurcation the continuum is assumed to yield plastically on both sides of the band at the onset of the instability; in discontinuous bifurcation the continuum is assumed to yield plastically inside the band and unload elastically outside the band. These two modes of bifurcation have been identified by Rudnicki and Rice (1975) and Rice and Rudnicki (1980). In a recent paper, Borja (2002a) showed that the two modes in fact will occur at the same time for the case of perfect plasticity.

For an elastic-perfectly plastic model a necessary condition for the inception of a shear band along a potential slip surface $\mathcal{S}$ is the vanishing of the determinant of the elastic-perfectly plastic acoustic tensor **A**, with components A_{jk}, and takes the form

$$\det(\mathbf{A})=0, \quad A_{jk}=n_i C^{ep}_{ijkl} n_l \tag{1}$$

where the n_i's=components of the unit normal vector **n** to the band, see Fig. 2. Here, the elastic-perfectly plastic moduli tensor C^{ep}_{ijkl} has the form

$$C^{ep}_{ijkl}=c^e_{ijkl}-\frac{1}{\chi}c^e_{ijpq}\frac{\partial Q}{\partial \sigma_{pq}}\frac{\partial F}{\partial \sigma_{rs}}c^e_{rskl}, \quad \chi=\frac{\partial F}{\partial \sigma_{ij}}c^e_{ijkl}\frac{\partial Q}{\partial \sigma_{kl}} \tag{2}$$

where σ_{ij}=Cauchy stress tensor. It must be noted that this result only applies to the case of infinitesimal deformation. In general, any result derived from such analysis must be taken with caution since geometric nonlinearities do play a very crucial role in the theory of bifurcation (Borja 2002b).

Since c^e_{ijkl} is positive definite, the determinant function

$$\mathcal{D}=\det(\mathbf{A}) \tag{3}$$

will approach zero from the positive side, assuming that the body is loaded from an initially elastic state (Runesson et al. 1991; Borja et al. 2000). The value of **n** at which the determinant function $\mathcal{D}$ vanishes for the first time defines the orientation of the surface of discontinuity $\mathcal{S}$, while the unit eigenvector **m** obtained from the eigenvalue problem (1) defines the instantaneous direction of the velocity jump vector at the onset of localization. In plane strain loading there are two possible orientations for $\mathcal{S}$; however, an algorithm for choosing the correct orientation can always be devised provided that the displacement gradient tensor at the onset of localization is nonsymmetric. If the displacement gradient tensor is symmetric, then no unique **n** can be chosen for the orientation of the band.

The onset of displacement jump damages a previously intact continuum and results in a bifurcated mechanical response, where the latter response is characterized by plastic deformation that is

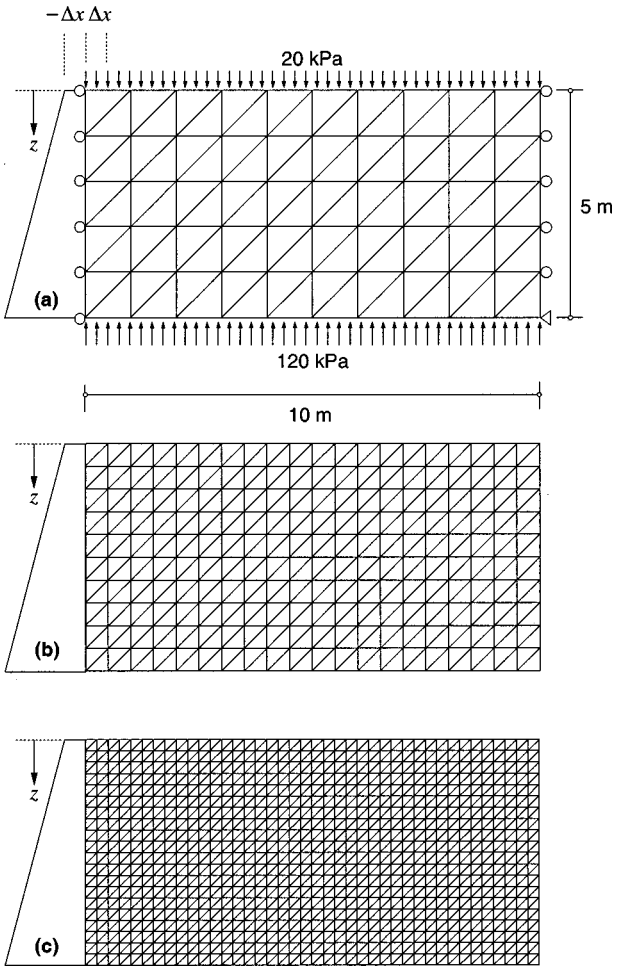

Fig. 3. FE meshes for plane strain localization analysis: (a) 100 elements; (b) 400 elements; (c) 1600 elements

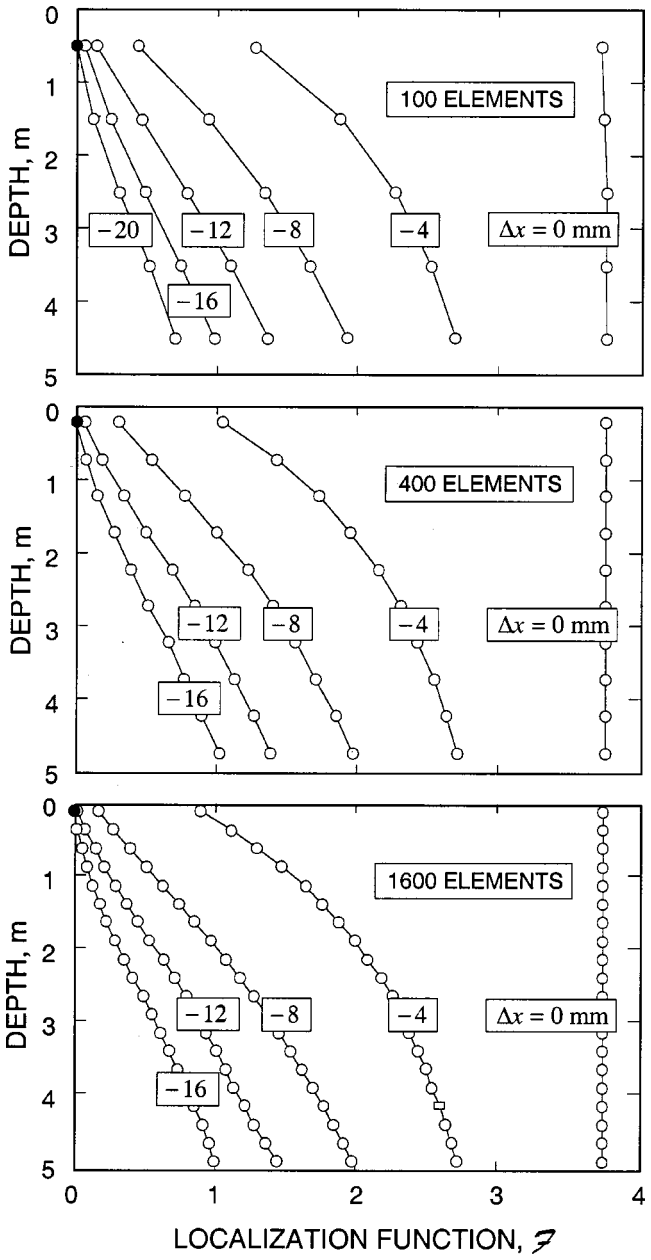

Fig. 4. Mesh convergence study: variation of localization function with depth, active case. Note: data points are evaluated at element centroids

now concentrated to the surface of discontinuity as the remaining part of the structure unloads elastically. Within the framework of small strain theory, the orientation vector **n** and the unit velocity jump vector **m** characterize the geometry of the plastic movement in the post-localization regime. It is useful to define a symmetric slip tensor **r**, with component r_{ij}, as

$$r_{ij} = \text{sym}(m_i n_j) = \tfrac{1}{2}(m_i n_j + m_j n_i) \tag{4}$$

where the symbol "sym" denotes a symmetrization operator. The tensor r_{ij} defines the plastic deformation on the band at post-post-localization (Borja and Regueiro 2001; Borja 2001), and has the same meaning as the plastic slip tensor used by Rice (1980) in seismic dislocation theory.

Yielding on the band is defined by a damage yield function G and a plastic potential function R. Here, the term "damage" refers to a break in a homogeneous pattern of deformation going into localized deformation. It must be noted that the functions G and R may be entirely different from the prelocalization functions F and Q; the latter functions pertain to the intact state whereas the former pertain to the bifurcated state. In this paper we assume that the prelocalization model represented by the functions F and Q is described by a nonassociated elastic-perfectly plastic Drucker-Prager model [see Borja et al. (2000) for the specific forms of these functions]. Setting the cohesion parameter equal to zero makes this model applicable to cohesionless granular materials.

Once an element satisfies the localization condition it could theoretically exhibit a bifurcated response, herein characterized by a damage function of the form

$$G = n_i \sigma_{ij} t_j - [c_{\mathcal{S}} - n_i \sigma_{ij} n_j \tan \phi_{\mathcal{S}}] = 0 \tag{5}$$

where t_j = component of unit vector **t** tangent to the band; $c_{\mathcal{S}}$ = mobilized cohesion on the band; and $\phi_{\mathcal{S}}$ = mobilized friction angle on the band. Note that Eq. (5) is nothing else but the standard Mohr–Coulomb law where $n_i \sigma_{ij} t_j$ = resolved shear stress on the surface of discontinuity $\mathcal{S}$, and $\tau_Y = c_{\mathcal{S}} - n_i \sigma_{ij} n_j \tan \phi_{\mathcal{S}}$ = yield shear resistance on $\mathcal{S}$ (the continuum mechanics convention is used in this equation). Obviously, for consistency with the prelocalization continuum model, the conditions $F = 0$ and $G = 0$ must be satisfied simultaneously at the onset of localization. However, since the mobilized friction angle $\phi_{\mathcal{S}}$ at residual state

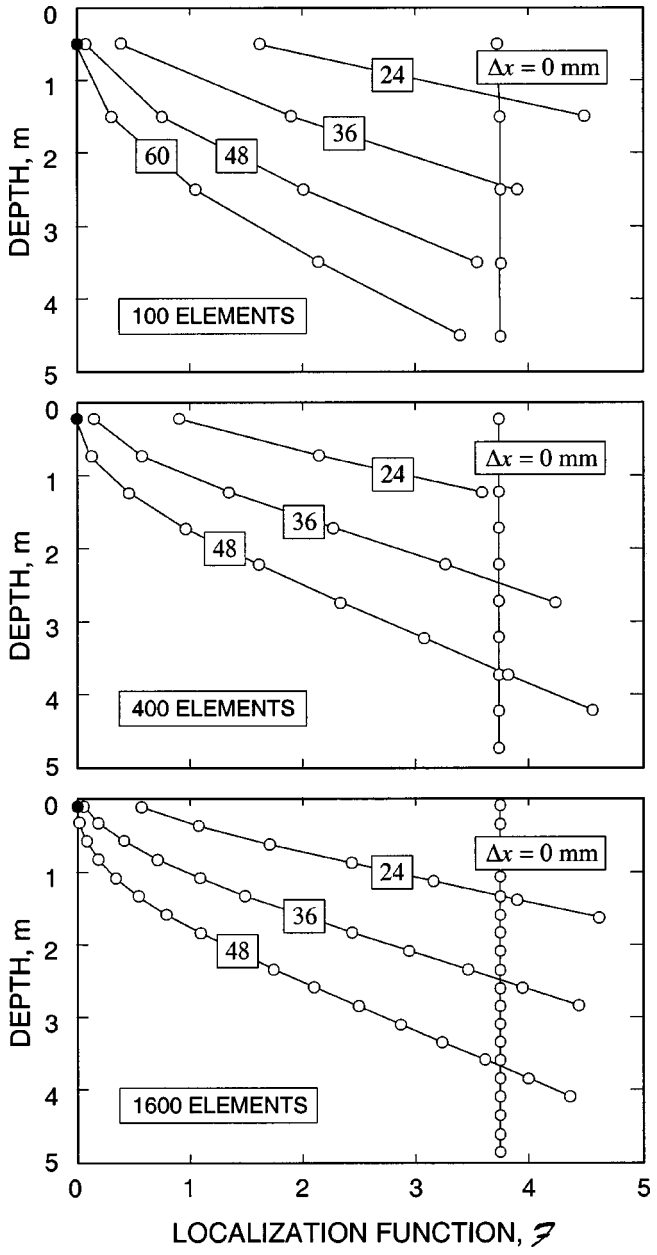

Fig. 5. Mesh convergence study: variation of localization function with depth, passive case. Note: data points are evaluated at element centroids

must be less than that prior to localization, it follows that the mobilized cohesion $c_{\mathcal{S}}$ right after localization must be greater than zero. Let us denote the value of the stress tensor at the onset of strong discontinuity by σ^*_{ij}; the condition $G=0$ at the onset of bifurcation gives

$$c_{\mathcal{S}}=n_i\sigma^*_{ij}t_j+n_i\sigma^*_{ij}n_j\tan\phi_{\mathcal{S}}>0 \tag{6}$$

This defines the initial value of $c_{\mathcal{S}}$ at the onset of localization.

A purely frictional response at residual state implies that the mobilized cohesion $c_{\mathcal{S}}$ on the band must decay to zero with increasing relative movement. This feature is captured by a cohesion softening law (Vermeer and de Borst 1984). The rate of cohesion softening is dictated by a plastic softening modulus $H_{\mathcal{S}}$. Here, we assume that the mobilized friction angle $\phi_{\mathcal{S}}$ is constant while the mobilized cohesion $c_{\mathcal{S}}$ decays to zero. It must be noted that for rocks the value of the mobilized angle of friction $\phi_{\mathcal{S}}$ on the surface of discontinuity could also vary with slip speed and some other state variables (Ruina 1983; Dieterich and Linker 1992; Dieterich and Kilgore 1994; Sleep 1997).

Numerical Simulations

We will restrict the simulations to the case of smooth retaining wall with a vertical backface and supporting an elastoplastic horizontal backfill. Three FE meshes of increasing degree of refinement are shown in Fig. 3. The meshes consist of 100, 400, and 1600 constant strain triangle (CST) elements, which are unstructured in the sense that no attempt was made to align element sides to expected orientation of the shear band. Vertical faces are supported on horizontal rollers, and the bases are supported by vertical tractions that balance the weight of the backfill and the surface load acting on top of the backfill. This is a slight departure from a conventional procedure of fixing the base of the mesh, which will not work in the present problem since the accompanying kinematical constraints will restrict the development of the shear band.

We assume the following material parameters for the cohesionless backfill prior to localization: Young's modulus $E=26\,000$ kPa; Poisson's ratio $\nu=0.3$; and Drucker–Prager parameters $\beta=0.4$ and $b=0.2$ [the notations are the same as those used by Borja et al. (2000)]. Assuming that the circular cone approximation passes through the inner corners of the Mohr-Coulomb hexagon, then the parameters β and b correspond to continuum friction and dilatancy angles $\bar{\phi}=23.1°$ and $\bar{\psi}=10.6°$, respectively. Note that the friction angle $\bar{\phi}$ corresponds to initial yielding and not to failure, and that the value of $\bar{\psi}$ represents the dilatancy angle for the intact continuum. The material parameters described above have been chosen on purpose so as to bring all gravity-induced stresses to yield condition even prior to active or passive loading.

Once the localization criterion is detected, the localizing element on the way of the shear band is enhanced to accommodate the presence of displacement jumps. In this case, the bifurcated yield strength is described by the mobilized cohesion $c_{\mathcal{S}}$ and mobilized friction angle $\phi_{\mathcal{S}}$, where the former is assumed to soften to zero at residual state while the latter is assumed to have a constant value $\phi_{\mathcal{S}}=22°$ throughout the bifurcated stage. The rate at which the mobilized cohesion softens to zero is dictated by the value of the softening modulus on the band, and for this example we assume $H_{\mathcal{S}}=-40$ kPa/m. In all simulations we have employed the standard Galerkin FE approximation with embedded discontinuity advocated by Borja (2000) to model the bifurcated response.

Slip-Line Tracing Algorithm

A slip-line tracing algorithm described in detail by Regueiro (1998) and Lai (2001) is used to track the propagation of strong discontinuity. In a nutshell, this algorithm classifies the elements as either ''intact,'' ''detected,'' or ''traced.'' Intact elements behave either elastically or plastically, and have yet to satisfy the localization condition. Intact elements are never enhanced. Detected elements behave plastically and have satisfied the localization condition, but have not yet been enhanced because the shear band has yet to cross them. It is possible for a detected element to remain unenhanced if it is not on the way of the shear band. Traced elements are detected elements that have been crossed by

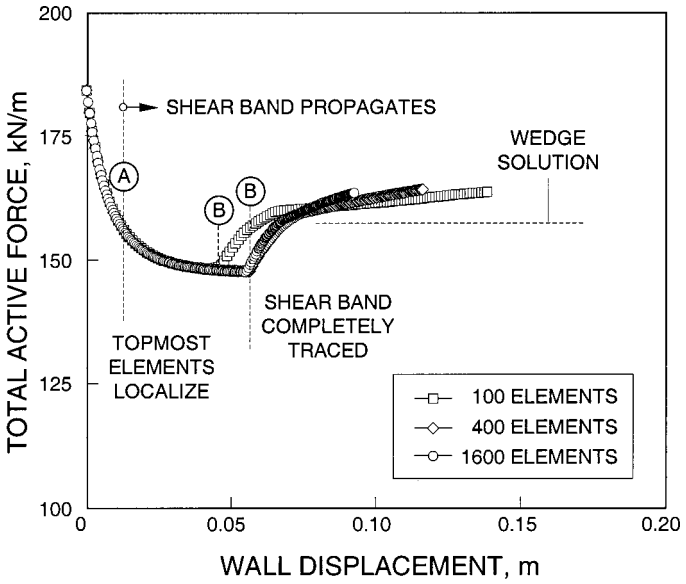

Fig. 6. Load-displacement curves for retaining wall problem: active loading

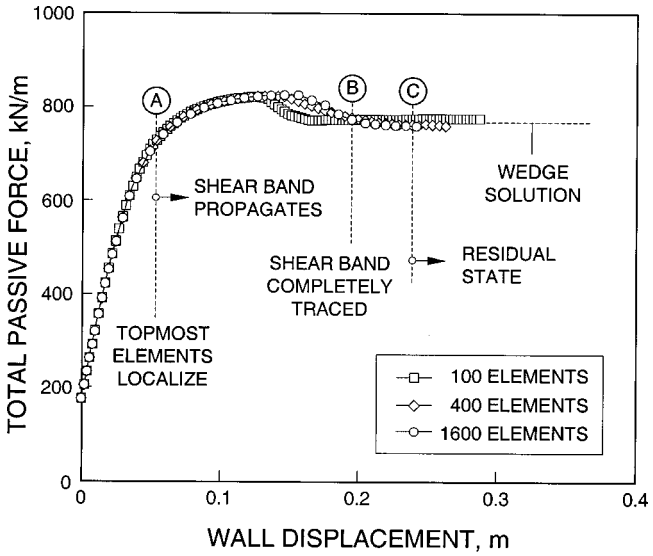

Fig. 8. Load-displacement curves for retaining wall problem: passive loading

the shear band, and have been enhanced to accommodate the presence of displacement jumps.

The slip-line tracing algorithm consists of three cases. The first case pertains to element which is first to localize. Here, slip line is traced through the element starting from a given element side location and at an orientation θ shown in Fig. 2. The second case pertains to an element adjacent to a traced element and sharing a side intersected by the tip of the slip line. Here, the slip line is traced across the newly localizing element at a current orientation θ starting at the slip-line intersection of the adjacent traced element. The third case pertains to element that is not adjacent to a traced element. In this case, the element is not traced even if it satisfied the localization condition. Note that it is possible to have multiple slip lines; in that case, there is more than one start element, but the tracing algorithm is the same. In the examples that follow, we will restrict the analyses to the case with only one slip line.

Initial Condition

Initial condition is first established by applying a downward gravity load of $\gamma = 20\,\text{kN/m}^3$, a downward surface load of $q = 20\,\text{kPa}$ (equivalent to 1 m surcharge), and an upward reactive load of 120 kPa to the meshes of Fig. 3. The surface load above

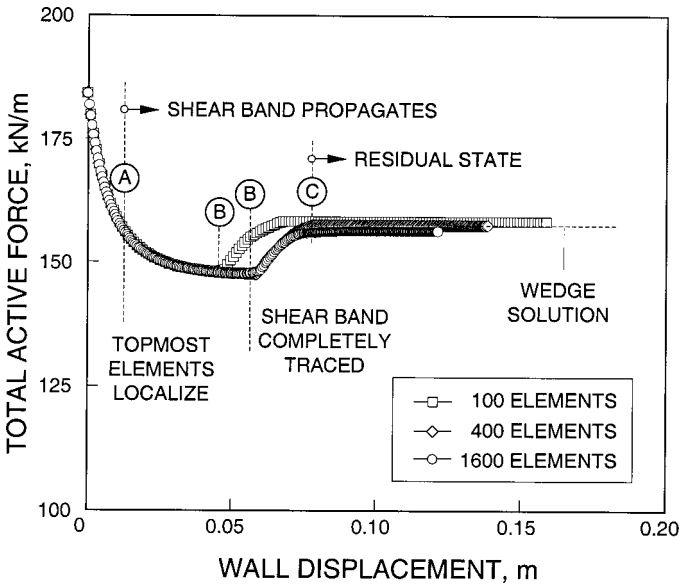

Fig. 7. Load-displacement curves for retaining wall problem: active loading with constant averaged shear band angle

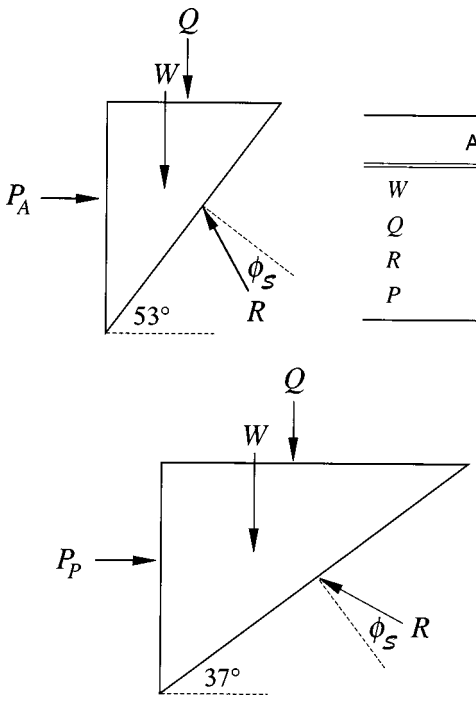

	ACTIVE	PASSIVE
W	188.4	331.8
Q	75.4	132.7
R	307.8	901.9
P	158.6	773.1

Fig. 9. Active and passive wedges at residual state. Notes: all forces in kN/m; failure plane orientations calculated from averaged shear band orientations

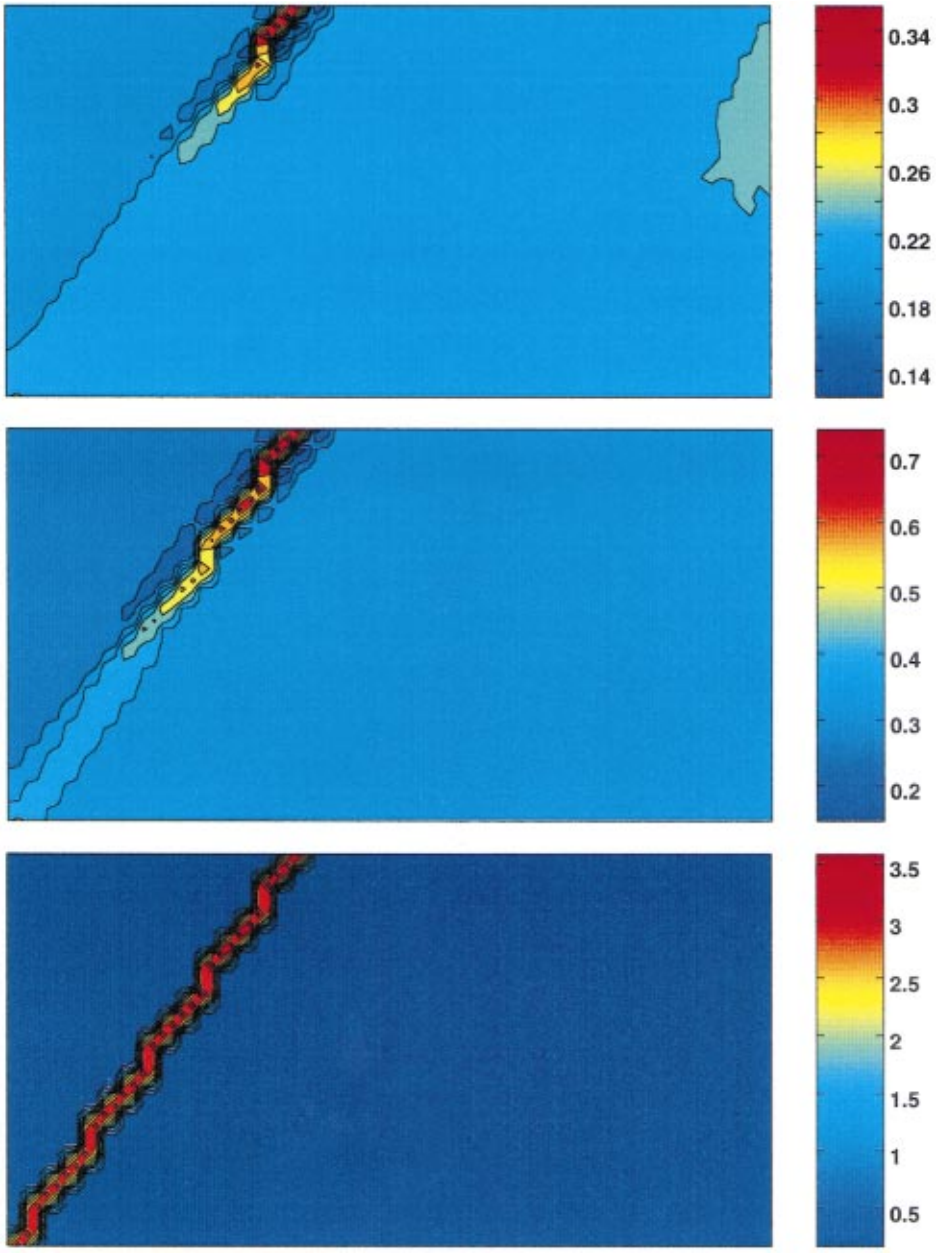

Fig. 10. Conforming octahedral shear strains showing different stages of shear band development: active case

the mesh is applied to bring the uppermost stress points sufficiently far from the origin of the stress space, thus avoiding complications with vertex effects induced by the yield surface. With this loading all initial stress points were brought to yield condition even prior to active or passive loading. Theoretically, stresses should vary only with depth from the ground surface, but some horizontal variations were also noted due to bias with orientation of the standard CST elements. This bias is of secondary importance and has been ignored in the present analysis.

For plane strain loading the determinant condition $\mathcal{D}=0$ is equivalent to the localization condition

$$\mathcal{F}=(1-\nu)\left(\frac{3\sqrt{2}s_3}{\sqrt{s_{ij}s_{ij}}}+\beta+b\right)^2-2(\beta-b)^2=0 \qquad (7)$$

where s_{ij} = deviatoric component of Cauchy stress tensor; s_3 = out-of-plane normal component of s_{ij}; and ν = Poisson's ratio. Variations of $\mathcal{F}$ with depth for the three meshes are plotted in Figs. 4 and 5, based on the stress values provided by the FE solutions. Note that, under the K_0 condition, $\mathcal{F}$ theoretically varies uniformly with depth (see plots labeled $\Delta x=0$ m in Figs. 4 and 5). Since $\mathcal{F}$ is nowhere near zero initially, it is not possible for any element to localize under K_0 loading (trivial result).

Onset of Strain Localization

For the active case the wall of Fig. 3 is moved horizontally to the left so that $\Delta x<0$. Fig. 4 plots contours of the localization function $\mathcal{F}$ as a function of wall movement. The figure clearly suggests a strong tendency for localization to initiate in the uppermost row of elements. Here, data points are denoted by open circles located at element centroids. The fact that $\mathcal{F}$ can be calculated at each element centroid implies that all stress points continue to yield plastically during active loading. Localization is first detected in the uppermost row of elements when the wall movement has reached a value $\Delta x=-20$ mm for the 100-element

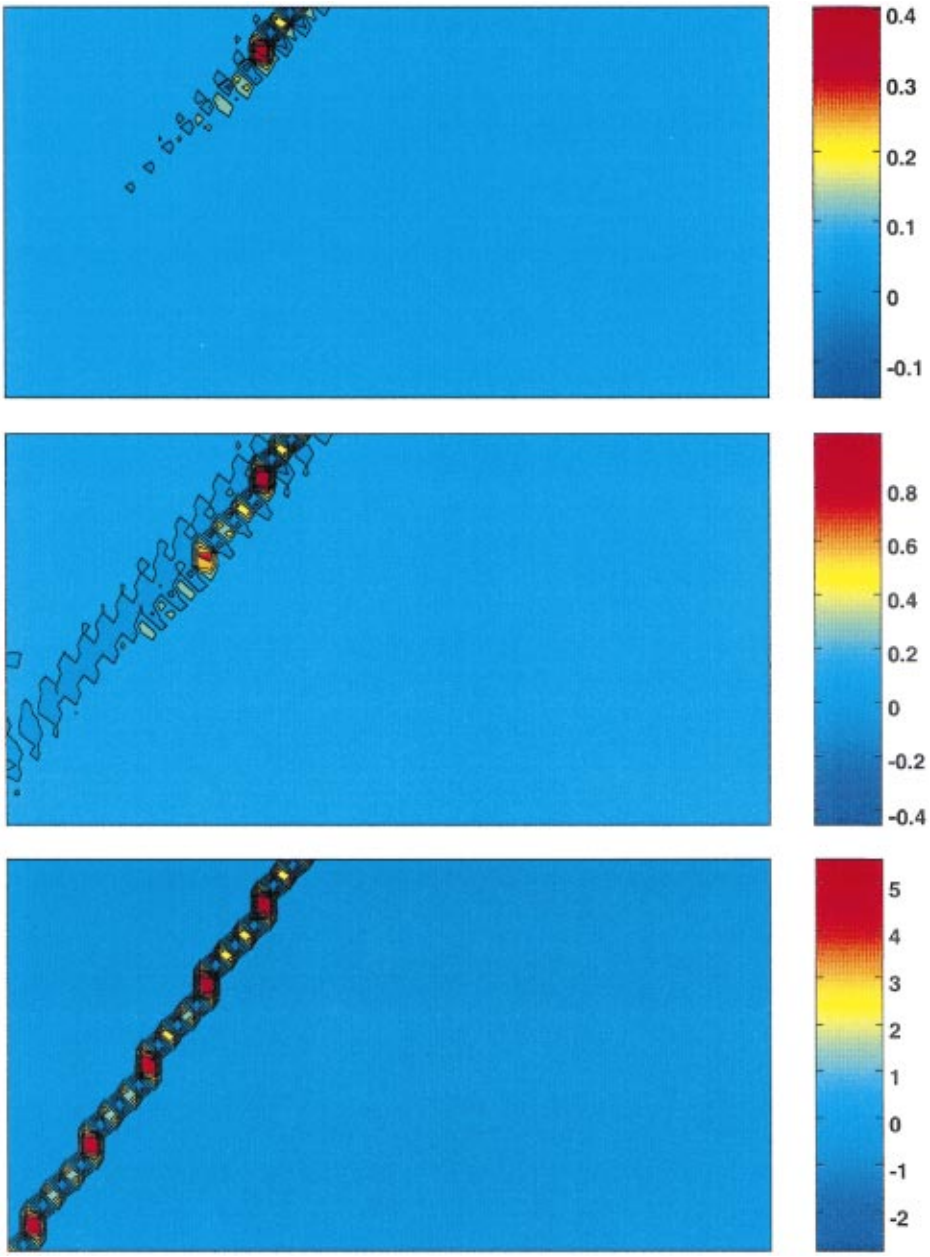

Fig. 11. Conforming volumetric strains showing different stages of shear band development: active case

mesh, and $\Delta x = -16$ mm for the 400- and 1600-element meshes (see dark circles). This suggests that the 100-element mesh is too coarse to capture the spatial variation of the localization function; however, convergence is easily achieved by refining meshes. Further wall movement causes the value of $\mathcal{F}$ to reverse in sign. Since the topmost elements localize simultaneously, no unique shear band position can be identified, implying that a potential shear band can initiate anywhere on the ground surface. For simulation purposes we prescribe a point on the ground surface from which the shear band initiates; this is equivalent to prescribing a weak element from which the slip line may be traced.

For passive loading the wall of Fig. 3 is moved horizontally to the right so that $\Delta x > 0$. Initially, this causes all elements behind the wall to unload elastically and come in contact with the opposite (compressional) side of the yield surface. At a wall movement of 24 mm, some elements within the upper soil layer have yielded plastically, allowing the localization function $\mathcal{F}$ to be calculated for those elements. At a wall movement of 60 mm for the 100-element mesh, and 48 mm for the 400- and 1600-element meshes, the topmost elements behind the retaining wall have yielded enough to satisfy the localization condition. Again, the 100-element mesh is too coarse to resolve the spatial variation of $\mathcal{F}$, but convergence is easily achieved by refining meshes. Further wall movement causes the values of $\mathcal{F}$ to reverse in sign.

Note that for the same material parameters it takes a larger wall movement to initiate a displacement jump in passive loading than it does to localize in active loading. Furthermore, note from the trends implied by the spatial variations of the localization function that with further loading the slip line is likely to propagate downward as the elements located at greater depths satisfy the localization condition.

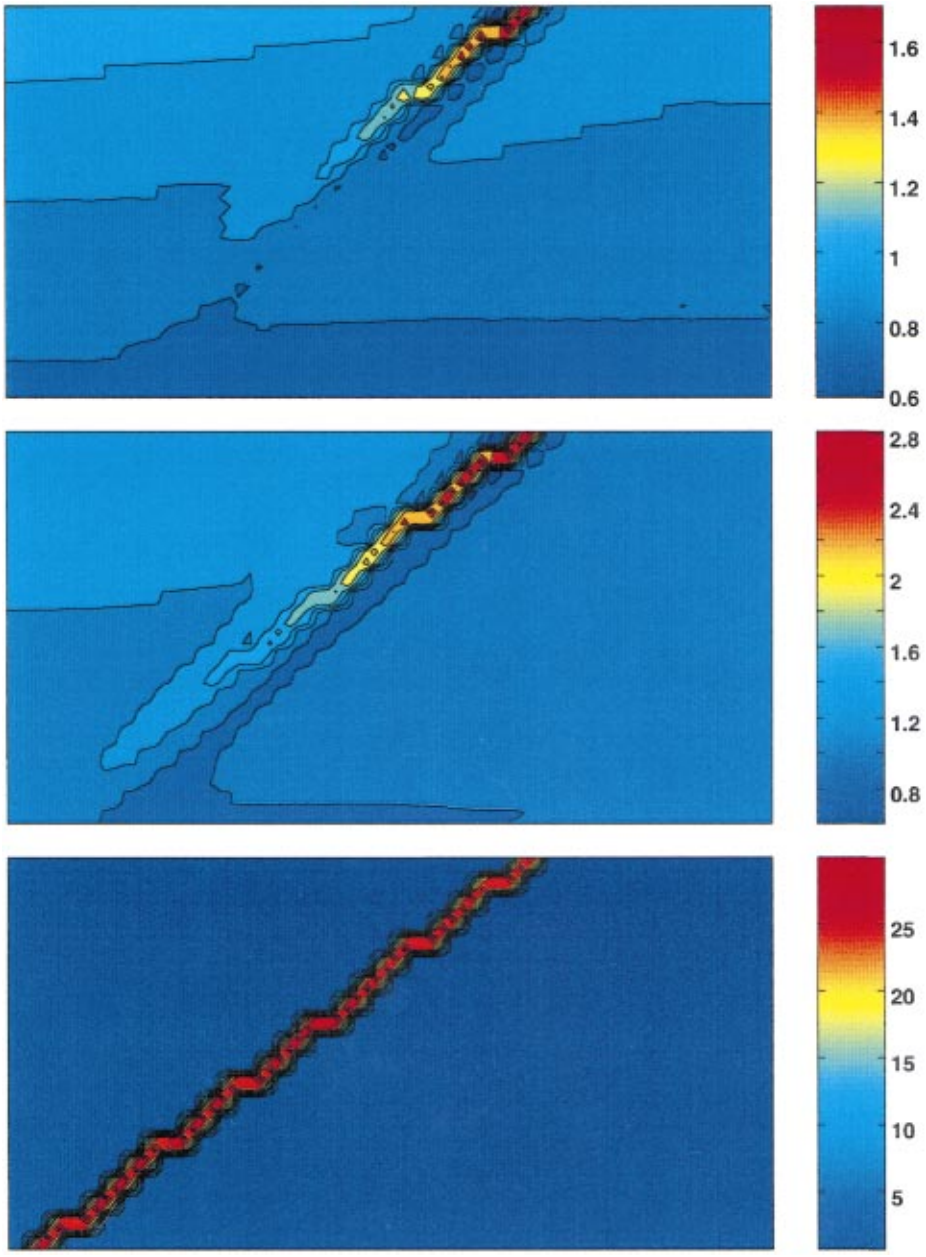

Fig. 12. Conforming octahedral shear strains showing different stages of shear band development: passive case

Propagation of Strong Discontinuity: Force-Displacement Responses

The soil response to active loading can be summarized with the aid of force-displacement curves shown in Fig. 6. Here, the wall reaction begins with an initial value of $K_0(\gamma H^2/2+qH) = 184$ kN/m and initially decreases with wall displacement, as expected. Localization of uppermost elements are detected at point *A*, after which a slip line is traced from a prescribed point on the ground surface in such a way that the shear band freely intersects the bottom boundary of the mesh. As the shear band propagates, the cohesion parameter c_S softens to zero on all traced elements. Slip-line tracing has been completed at point *B* when the shear band intersected the bottom boundary of the mesh. Note that the algorithm traces the shear band slightly sooner with the 100-element mesh, again because this mesh is too coarse for the problem at hand.

After the slip line has been completely traced, cohesion softening accelerates following point *B*, bringing the slip-line forces to the residual state. Theoretically, the residual state is characterized by a plateau in the load-displacement plots, but the active forces continue to increase as the elements surrounding the shear band begin to yield as a continuum. This is due to the generally curved shear band that formed, whose orientations vary from about 50° to 55° from the horizontal. A curved shear band inhibits a free kinematical movement of the active wedges and prevents the development of a true residual state.

To illustrate the effect of the nonconstancy of the shear band orientation, a slight variation to the slip-line tracing algorithm described above has been explored. Here, the individual slip-line orientations obtained previously have been averaged, and this averaged value (53° relative to the horizontal) was used to define uniform slip-line orientations for all traced elements. Essentially,

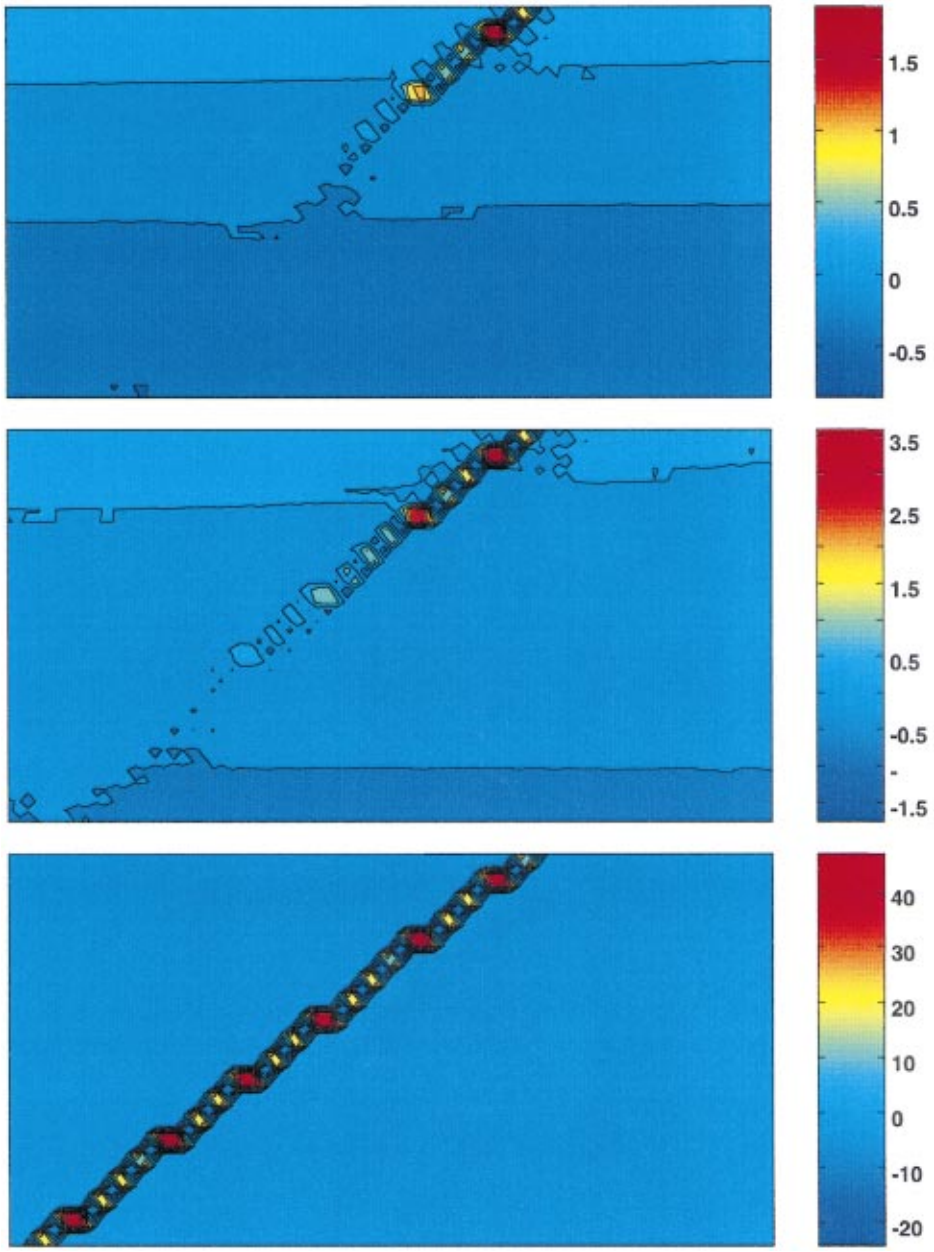

Fig. 13. Conforming volumetric strains showing different stages of shear band development: passive case

this forces the surface of discontinuity to be a straight line. Fig. 7 shows the results of the modified simulations and indicates that the load-displacement responses now exhibit constant wall reactions at residual state. The shape of the force-displacement responses portrayed in Figs. 6 and 7 for the active case is consistent with a well-known trend exhibited by a retaining wall supporting an initially dense granular backfill (Design Manual 1971).

For passive loading the load-displacement responses are shown in Fig. 8. Starting from the same initial wall reaction of 184 kN/m the passive forces first increase with wall movement. Then, the topmost elements localize at point *A* when the wall has moved by about 0.05 m toward the backfill (cf. Fig. 5). A shear band then emerges and is traced starting from a prescribed point on the ground surface in such a way that the slip line freely intersects the bottom boundary of the mesh. In this example, the computed shear band orientations vary from about 36° to 41°, with an averaged value of 37° relative to the horizontal. An overall softening response follows until the shear band has been completely traced, and even beyond this point. Like the active case, a curved shear band did not allow the development of a true residual state; nevertheless, the wall reactions appear to have stabilized enough to a constant value.

A limit equilibrium-type of solution is useful for checking the final results provided by the FE localization model. Simple calculations based on the wedge method, and using the averaged slip-line orientations (53° from the horizontal for active, and 37° for passive) to define the geometry of the wedges, are performed in Fig. 9 for both active and passive loading. Note that these averaged shear band orientations agree better with the expression $45° \pm (\bar{\phi} + \bar{\psi})/4$ from the horizontal, as suggested by Arthur et al. (1977), than to either the expression $45° \pm \bar{\phi}/2$, or $45° \pm \bar{\psi}/2$. The total wall reactions calculated in Fig. 9 (158.6 kN/m for the active case and 773.1 kN/m for the passive case) agree well with the

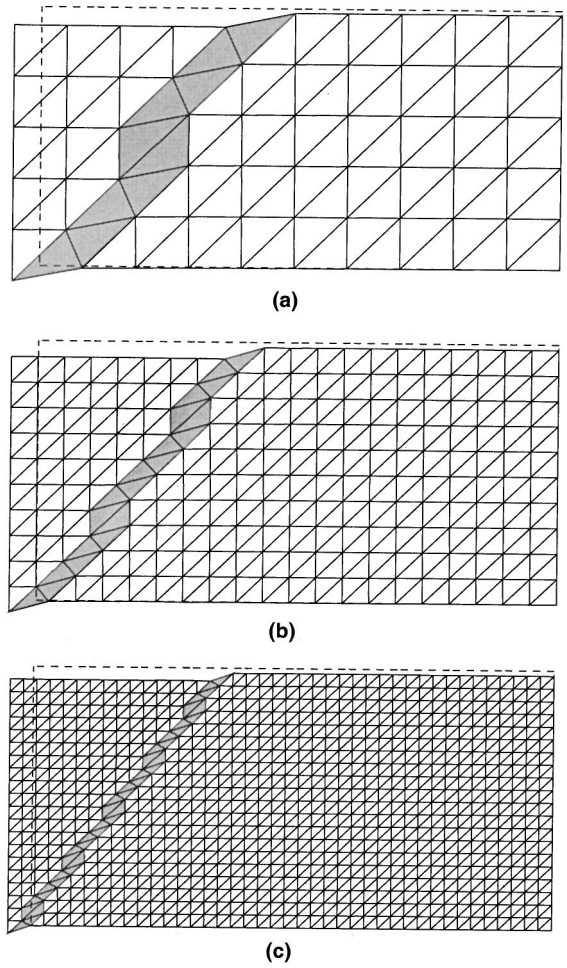

Fig. 14. Deformed meshes at end of active loading: (a) 100 elements; (b) 400 elements; (c) 1600 elements (displacement magnification = 5; final horizontal displacement = −0.10 m)

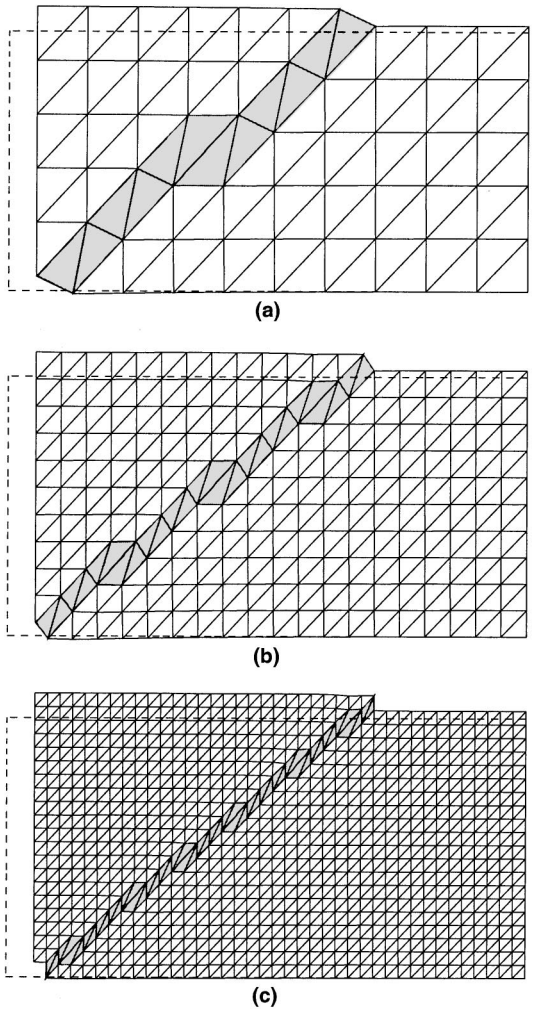

Fig. 15. Deformed meshes at end of passive loading: (a) 100 elements; (b) 400 elements; (c) 1600 elements (displacement magnification = 2; final horizontal displacement = 0.27 m)

''residual state'' values predicted by the localization model, and are sketched as horizontal dashed lines in Figs. 6–8.

Conforming Octahedral Shear and Volumetric Strains

Conforming strains are calculated by interpolating the total nodal displacements provided by the FE solution using the standard strain-displacement operator matrix **B**. For CST elements not traced by a shear band, the conforming strains are piecewise constant and discontinuous across element boundaries. For elements traced by a shear band the conforming strains represent only part of the total strains, the ''enhanced strains'' representing the other part (Simo et al. 1993). Since the total strains are singular on the shear band where jumps in the displacement field take place, it follows that the enhanced part contains the singularities resulting from the displacement jumps. Contour plots of conforming strains are useful in assessing the effect of the shear band on the deformation patterns in neighboring elements, as well as in predicting what direction the shear band is heading. In this section we present contour plots of conforming octahedral shear and volumetric strains at different stages of shear band development for both active and passive loading.

For the active case contour plots of conforming octahedral shear and volumetric strains (in percent) are shown in Figs. 10 and 11, respectively. Here, the specific shear band of interest emanates from the ground surface at a prescribed point located approximately at a distance of 3.9 m behind the wall. Theoretically, the shear band can have two possible orientations—either going toward, or away from the wall; however, the orientations of CST elements favored the development of a shear band that goes toward the wall. The strain contours shown in Figs. 10 and 11 show different stages of shear band development, at about 1/3, 2/3, and full development, or stages 1, 2, and 3, respectively. These plots have been constructed using solutions from the 1600-element mesh. Clearly, the contours shown in Figs. 10 and 11 are indicative of the effect of the displacement jumps on the overall deformation pattern in the mesh. For example, the stage 1 contours clearly suggest where the shear band is heading if the wall continues to move away from the soil.

For the passive case contour plots of conforming octahedral shear and volumetric strains (in percent) are shown in Figs. 12 and 13, respectively. These plots were also generated from the 1600-element mesh. Here, the specific shear band of interest emanates from a point located approximately at a distance of 6.9 m behind the wall, and propagating downward toward the wall. Observe from stages 1 and 2 propagation that the deeper elements are less deformed than the shallower ones, but as the band fully develops the deformation becomes more and more concentrated

to the surface of discontinuity. Plastic dilatancy on the band is noted throughout the simulations, in agreement with observed behavior of most rocks and dense sands (Brace et al. 1966; Cook 1970; Vardoulakis and Graf 1985).

Deformed meshes at the conclusion of the simulations are shown in Figs. 14 and 15 for the active and passive cases, respectively. The shear band orientations are nearly the same for each case, regardless of the mesh, and irrespective of the fact that the meshes are unstructured in the sense that the element sides are not necessarily aligned to the shear bands. Unlike the results reported in a similar paper (Borja et al. 2000) where mesh independence to machine precision was achieved with the FE solutions, it was not possible to achieve such a high level of accuracy in the present simulations due to the numerical errors associated with the slip-line tracing procedure [the simulations presented by Borja et al. (2000) involved bifurcations from a homogeneous stress state and did not necessitate any special slip-line tracing technique since all the elements have localized at the same time]. However, mesh dependence was not a critical issue in the present simulations particularly with the solutions from the 400- and 1600-element meshes.

Remarks on Numerical Model and Results

Conforming strains in the traced elements may appear very high, but, again, one must add the enhanced part to obtain the total strains. Once this is done, the values of the total strains in the traced elements become comparable in magnitude to those of the much less deformed neighboring elements, except on the surface of discontinuity itself where the total strain is singular. Since the total strains are small everywhere except on the surface of discontinuity, a small strain formulation is still acceptable even if the conforming strains appear very high. Furthermore, as the mesh becomes finer and finer the apparent thickness of the shear band in Figs. 10–15 reduces to zero. However, an extremely fine mesh is not required by the model because the FE formulation is capable of handling just as accurately the effect of displacement jumps even with a relatively coarse mesh.

As to the limitations of the analyses, we have assumed throughout that the horizontal and vertical axes coincide with the principal stress directions, so, in effect the specific problem addressed in this paper has no dimension. In fact, even the height of the retaining wall has been used only as an artificial parameter. Frictional effects at the base and other details of the boundary conditions such as wall rotation have been ignored. In general, boundary conditions do influence the initiation and propagation of shear bands and must be captured accurately in a true boundary-value problem. Work is underway dealing with shear strain localization behind a geosynthetic-reinforced soil wall investigating how boundary condition effects influence the initiation and propagation of shear bands.

Summary and Conclusions

A recently developed strain localization FE model has been used to investigate the propagation of strong discontinuity in elastoplastic solids subjected to active and passive loading. The analyses apply to dilative frictional materials susceptible to shear banding. Results of the analyses show that for a homogeneous elastoplastic backfill displacement jump first emerges on the ground surface, and then with continued wall movement strong discontinuity propagates downward at an angle that depends on the state of stress—active or passive—at the onset of localization. This contrasts with the Rankine theory which states that failure at all points occurs simultaneously in a loose, homogeneous, granular backfill.

The simulations replicate a well-known result that active loading requires a smaller movement to develop a displacement jump as compared to passive loading. Separate parametric studies not presented in this article suggest that these conclusions are valid not only for the specific set of material data used in the present simulations, but also for a wider range of realistic material parameter values. Work is underway involving shear strain localization behind a geosynthetic-reinforced soil wall to investigate the robustness of the model for solving more realistic boundary-value problems.

Acknowledgments

Financial support for this research was provided by the G3S Division of National Science Foundation under Contract No. CMS-9700426. The writers gratefully acknowledge this support.

References

Adachi, T., Oka, F., and Yashima, A. (1991). ''A finite element analysis of strain localization for soft rock using a constitutive equation with strain softening.'' *Arch. Appl. Mech.*, 61, 183–191.

Armero, F., and Garikipati, K. (1995). ''Recent advances in the analysis and numerical simulation of strain localization in inelastic solids.'' *Proceedings of Computational Plasticity IV*, D. R. J. Owen, E. Oñate, and E. Hinton, eds., International Center for Numerical Methods in Engineering, Barcelona, Spain, 547–561.

Arthur, J. R. F., Dunstan, T., Al-ani, Q. A. L. J., and Assadi, A. (1977). ''Plastic deformation and failure in granular media.'' *Géotechnique*, 27, 53–74.

Aydin, A., and Johnson, A. M. (1978). ''Development of faults as zones of deformation bands and as slip surfaces in sandstone.'' *Pure and Applied Geophysics*, 116, 931–942.

Bazant, Z. P., and Pijaudier-Cabot, G. (1988). ''Nonlocal continuum damage, localization instability and convergence.'' *J. Appl. Mech.*, 55, 287–293.

Borja, R. I. (2000). ''A finite element model for strain localization analysis of strongly discontinuous fields based on standard Galerkin approximation.'' *Comput. Methods Appl. Mech. Eng.*, 190(11–12), 1529–1549.

Borja, R. I. (2001). ''Propagation of strong discontinuity in elastoplastic solids.'' *Computer methods and advances in geomechanics*, Vol. 1, C. S. Desai et al., eds., Balkema, Rotterdam, 491–495.

Borja, R. I. (2002a). ''Bifurcation of elastoplastic solids to shear band mode at finite strain.'' *Comput. Methods Appl. Mech. Eng.*, in press.

Borja, R. I. (2002b). ''Finite element simulation of strain localization with large deformation: Capturing strong discontinuity using a Petrov-Galerkin multiscale formulation.'' *Comput. Methods Appl. Mech. Eng.*, in press.

Borja, R. I., and Regueiro, R. A. (2001). ''Strain localization in frictional materials exhibiting displacement jumps.'' *Comput. Methods Appl. Mech. Eng.*, 190(20–21), 2555–2580.

Borja, R. I., Regueiro, R. A., and Lai, T. Y. (2000). ''FE modeling of strain localization in soft rocks.'' *J. Geotech. Geoenviron. Eng.*, 126(4), 335–343.

Brace, W. F., Paulding, B. W., and Scholz, C. (1966). ''Dilatancy in the fracture of crystalline rocks.'' *J. Geophys. Res.*, 71(16), 3939–3953.

Cook, N. G. W. (1970). ''An experiment proving that dilatancy is a pervasive volumetric property of brittle rock loaded to failure.'' *Rock Mech.*, 2, 181–188.

de Borst, R., and Mühlhaus, H.-B. (1992). ''Gradient-dependent plasticity: Formulation and algorithmic aspects.'' *Int. J. Numer. Methods Eng.*, 35, 521–539.

de Borst, R., Pamin, J., and Sluys, L. J. (1995). ''Computational issues in gradient plasticity.'' In: *Continuum models for materials with microstructures*, H. B. Mühlhaus, ed., Wiley, N.Y., 159–200.

Design Manual DM-7 (1971). *Soil mechanics, foundations, and earth structures*, Dept. of the Navy, Naval Facilities Engineering Command, Alexandria, VA.

Dieterich, J. H., and Kilgore, B. D. (1994). ''Direct observation of frictional contacts: New insights for state-dependent properties.'' *Pure and Applied Geophysics*, 143(1/2/3), 283–302.

Dieterich, J. H., and Linker, M. F. (1992). ''Fault stability under conditions of variable normal stress.'' *Geophys. Res. Lett.*, 19(16), 1691–1694.

Labuz, J. F., Dai, S. T., and Papamichos, E. (1996). ''Plane-strain compression of rocklike materials.'' *Int. J. Rock Mech. Min. Sci. Geomech. Abstr.*, 33, 573–584.

Lai, T. Y. (2001). ''FE modeling of post-localization behavior of elastoplastic solids with strong discontinuity.'' PhD thesis, Stanford University, Stanford, Calif.

Larsson, R., Runesson, K., and Ottosen, N. S. (1993). ''Discontinuous displacement approximation for capturing plastic localization.'' *Int. J. Numer. Methods Eng.*, 36, 2087–2105.

Oka, F., Yashima, A., Sawada, K., and Aifantis, E. C. (2000). ''Instability of gradient-dependent elastoviscoplastic model for clay and strain localization analysis.'' *Comput. Methods Appl. Mech. Eng.*, 183, 67–86.

Ortiz, M., Leroy, Y., and Needleman, A. (1987). ''A finite element method for localized failure analysis.'' *Comput. Methods Appl. Mech. Eng.*, 61, 189–214.

Perić, D., Runesson, K., and Sture, S. (1992). ''Evaluation of plastic bifurcation for plane strain versus axisymmetry.'' *J. Eng. Mech.*, 118(3), 512–524.

Perić, D., Runesson, K., and Sture, S. (1993). ''Prediction of plastic localization using MRS-Lade model.'' *J. Geotech. Eng.*, 119(4), 639–661.

Pietruszczak, S. T., and Mróz, Z. (1981). ''Finite element analysis of deformation of strain-softening materials.'' *Int. J. Numer. Methods Eng.*, 17, 327–334.

Rankine, W. J. M. (1857). ''On the stability of loose earth.'' *Philos. Trans. R. Soc. London*, 147(1), 9–27.

Read, H. E., and Hegemier, G. A. (1984). ''Strain softening of rock, soil and concrete—A review article.'' *Mech. Mater.*, 3, 271–294.

Regueiro, R. A. (1998). ''Finite element analysis of strain localization in geomaterials taking a strong discontinuity approach,'' PhD thesis, Stanford University, Stanford, Calif.

Regueiro, R. A., and Borja, R. I. (1999). ''A finite element model of localized deformation in frictional materials taking a strong discontinuity approach.'' *Finite Elem. Anal. Design*, 33(4), 283–315.

Regueiro, R. A., and Borja, R. I. (2001). ''Plane strain finite element analysis of pressure-sensitive plasticity with strong discontinuity.'' *Int. J. Solids Struct.*, 38, 3647–3672.

Rice, J. R. (1980). ''Elastic wave emission from damage processes.'' *J. Nondestruct. Eval.*, 1, 215–224.

Rice, J. R., and Rudnicki, J. W. (1980). ''A note on some features of the theory of localization of deformation.'' *Int. J. Solids Struct.*, 16, 597–605.

Rudnicki, J. W., and Rice, J. R. (1975). ''Conditions for the localization of deformation in pressure-sensitive dilatant materials.'' *J. Mech. Phys. Solids*, 23, 371–394.

Rudnicki, J. W. (1977). ''The inception of faulting in a rock mass with a weakened zone.'' *J. Geophys. Res.*, 82(5), 844–854.

Ruina, A. (1983). ''Slip instability and state variable friction laws.'' *J. Geophys. Res.*, 88, 10 359–10 370.

Runesson, K., Perić, D., and Sture, S. (1991). ''Discontinuous bifurcations of elastic–plastic solutions at plane stress and plane strain.'' *Int. J. Plast.*, 7, 99–121.

Simo, J. C., Oliver, J., and Armero, F. (1993). ''An analysis of strong discontinuities induced by strain-softening in rate-independent inelastic solids.'' *Comput. Mech.*, 12, 277–296.

Sleep, N. H. (1997). ''Application of a unified rate and state friction theory to the mechanics of fault zones with strain localization.'' *J. Geophys. Res.*, 102(B2), 2875–2895.

Vardoulakis, I., and Graf, B. (1985). ''Calibration of constitutive models for granular materials using data from biaxial experiments.'' *Géotechnique*, 35(3), 299–317.

Vermeer, P. A., and de Borst, R. (1984). ''Nonassociated plasticity for soils, concrete, and rock.'' *Heron*, 29(3), 1–64.

Viggiani, G., Finno, R. J., and Harris, W. W. (1994). ''Experimental observations of strain localisation in plane strain compression of a stiff clay.'' *Localization and bifurcation theory for soils and rocks*, R. Chambón, J. Desrues, and I. Vardoulakis, eds., Balkema, Rotterdam, The Netherlands, 189–198.

Wan, R. G., Chan, D. H., and Morgenstern, N. R. (1980). ''A finite element method for the analysis of shear bands in geomaterials.'' *Finite Elem. Anal. Design*, 7, 129–143.

Zienkiewicz, O. C., Pastor, M., and Huang, M. (1995). ''Softening, localisation and adaptive remeshing. Capture of discontinuous solutions.'' *Comput. Mech.*, 17, 98–106.